# Chapter-6

***(The effect of mechanochemically activated MgO in $Al_2O_3$–MgO–C)***

***Chapter 6***

# The effect of mechanochemically activated MgO in $Al_2O_3$–MgO–C

## 6.1 Motivation

$Al_2O_3$-MgO-C is increasingly being used in refractories for secondary steelmaking especially for ladle applications due to their particular combination of resistance to slag corrosion, high thermal shock resistance, and excellent hot strength. $Al_2O_3$-spinel refractories usually show better thermal shock/spalling resistance than MgO-spinel refractories as the difference in thermal expansion coefficients of the former is lower than later. M. Bavand-Vandchali et al., 2009, suggest the nature of *in situ* spinel in $Al_2O_3$-MgO-C refractory matrix produces an interlocking texture, which holds the graphite flakes within and improves the structural integrity. In this type of skeletal structure, the graphite and antioxidants can be confidently increased for getting better wear resistance.

A graphite content of the order of 6 wt% in the refractory matrix apparently helps build an appropriate set of thermo-mechanical properties and higher corrosion resistance, due to the low thermal expansion coefficient, high thermal conductivity, high refractoriness and a non-wettability by the slag. The refractory containing coarser MgO grains usually present reduced corrosion behavior, owing to the higher residual expansion, which helps the physical slag infiltration. Nonetheless, in an expansion controlled conditions, the

penetration indexes were reduced as a result of the lower volume of pores and flaws closure in the refractory microstructure.

Although the abrasion and corrosion resistance is one of the chief requisites for refining ladles, conclusive statements about the contents of *in situ* spinelization in AMC have not been reported. Considering this aspect, the primary aim of this work was to obtain an optimum content of *in situ* spinel for high thermo-mechanical properties. A fine mechanochemically activated MgO was varied 0-10 wt% in AMC refractory.

## 6.2 Formulation

| Raw Materials | AMC1 | AMC2 | AMC3 | AMC4 | AMC5 | AMC6 |
|---|---|---|---|---|---|---|
| **WFA (0.2-3mm)** | 72 | 72 | 72 | 72 | 72 | 72 |
| **Reactive alumina (74-44µ)** | 15 | 13 | 11 | 9 | 7 | 5 |
| **MgO (44µ)** | 0 | 2 | 4 | 6 | 8 | 10 |
| **Flaky Graphite** | 7 | 7 | 7 | 7 | 7 | 7 |
| **Resol** | 3.50 | 3.50 | 3.50 | 3.50 | 3.50 | 3.50 |
| **Powder Resin** | 0.50 | 0.50 | 0.50 | 0.50 | 0.50 | 0.50 |
| **NCB** | 1.0 | 1.0 | 1.0 | 1.0 | 1.0 | 1.0 |
| **Al-Metal Powder** | 0.50 | 0.50 | 0.50 | 0.50 | 0.50 | 0.50 |
| **$B_4C$** | 0.50 | 0.50 | 0.50 | 0.50 | 0.50 | 0.50 |

**Table 6.1** Incremental mechanically activated magnesia in $Al_2O_3$-MgO-C

The present composition has an increasing amount of mechanically activated magnesia in the matrix. The formulation AMC1 does not contain any magnesia and later on the content of magnesia is incremented 2 wt% in each fore coming specimen. AMC6 contains the highest magnesia content (10 wt%).

## 6.3 Results and Discussion

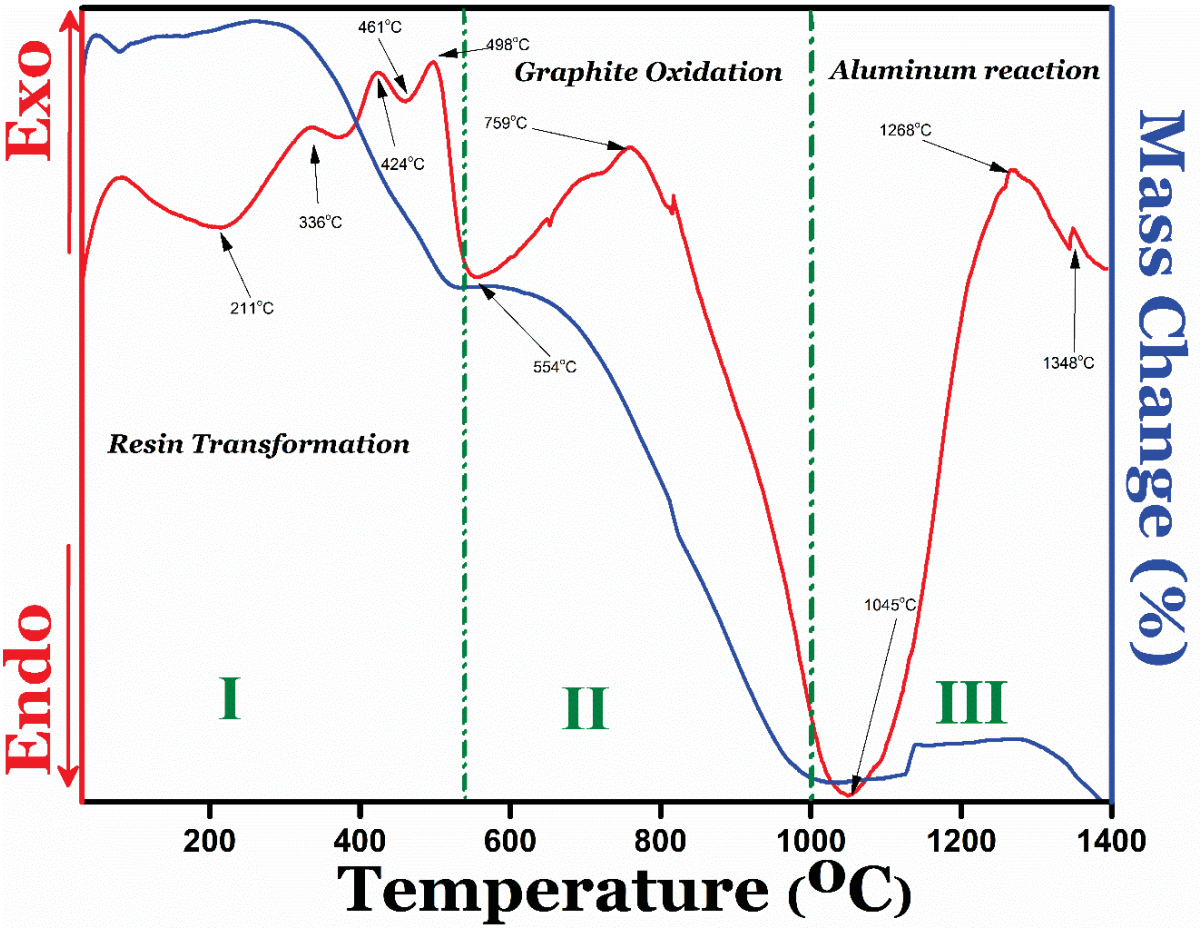


**Fig 6.1** Thermal evolution of AMC4 specimen

The thermograms acquired by DTA -TGA of AMC4 is shown in the above figure. The DTA plots show peaks between 200 and 580 °C that are ascribed to the resin transformation and residual carbon (glassy-carbon) oxidation around 554 °C. However, the resin pyrolysis temperature is also affected by the existence of diverse inorganic components. Weight loss accompanies both processes concerning the resin carbonization and the oxidation of the residual carbon due to the evolution of gases.

| Temperature | Process |
|---|---|
| **211°C (en)**<br>**336°C (ex)**<br>**424°C (ex)**<br>**461°C (en)**<br>**498°C (ex)**<br>**554°C (en)** | Resin Transformation |
| **652°C (en)** | Aluminium melting |
| **759°C (ex)** | Graphite Oxidation |
| **1045°C (en)** | Formation of $Al_4C_3$ |
| **1268°C (ex)** | Formation of $Al_2O_3$ ($Al_4C_3$ + $CO/O_2$) formation of spinel MgO. $Al_2O_3$ ($Al_2O_3$/Al(l) + MgO/Mg(g)) |
| **1351°C (ex)** | Formation of $Al_4O_4C$ |

**Table 6.2** Processes involving the thermal profile

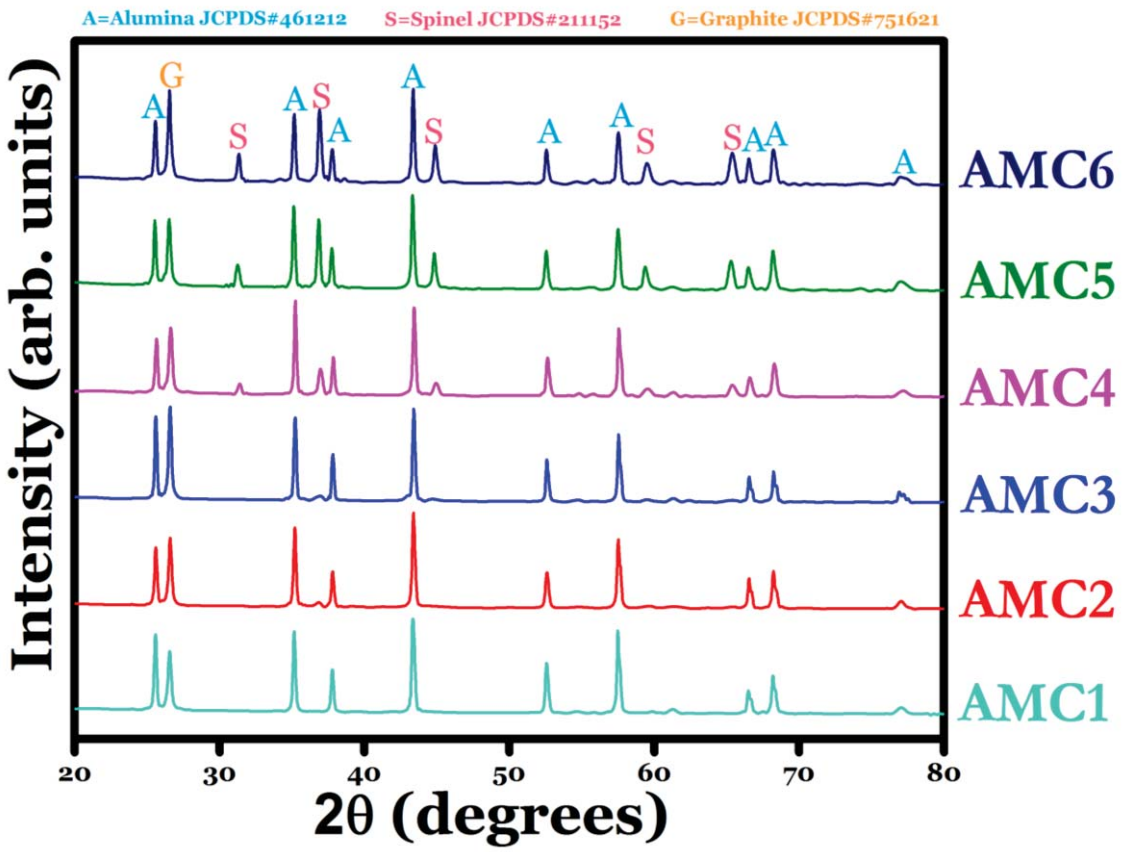


**Fig 6.2** XRD analysis of AMC sample coked at 1400°C with 3h soaking.

| Sample code | Crystallite size (D) nm | | | Dislocation density (δ) line²/m² (×10¹⁵) | | | Microstrain ε (×10⁻³) | | |
|---|---|---|---|---|---|---|---|---|---|
| | $Al_2O_3$ | $MgAl_2O_4$ | Graphite | $Al_2O_3$ | $MgAl_2O_4$ | Graphite | $Al_2O_3$ | $MgAl_2O_4$ | Graphite |
| AMC1 | 38 | ---- | 30.55 | 0.671 | ---- | 1.071 | 0.897 | ---- | 1.134 |
| AMC2 | 39 | 34 | 27 | 0.637 | 3.251 | 0.834 | 0.875 | 1.975 | 1.001 |
| AMC3 | 45 | 28 | 36 | 0.485 | 12.898 | 0.736 | 0.763 | 3.935 | 0.940 |
| AMC4 | 46 | 23 | 31 | 0.462 | 1.804 | 0.984 | 0.744 | 1.472 | 1.087 |
| AMC5 | 39 | 32 | 32 | 0.640 | 0.926 | 0.925 | 0.876 | 1.054 | 1.054 |
| AMC6 | 42 | 33 | 34 | 0.552 | 0.880 | 0.821 | 0.814 | 1.028 | 0.992 |

**Table 6.3** Crystallite size, dislocation density, and microstrain

| Sample Code | Relative crystallinity % | | |
|---|---|---|---|
| | $Al_2O_3$ | $MgAl_2O_4$ | Graphite |
| AMC1 | 89.15 | ------ | 10.85 |
| AMC2 | 87.66 | 4.54 | 11.80 |
| AMC3 | 75.64 | 10.76 | 13.60 |
| AMC4 | 67.59 | 21.86 | 10.55 |
| AMC5 | 65.06 | 26.89 | 8.05 |
| AMC6 | 55.37 | 34.90 | 9.71 |

**Table 6.4** Relative crystallinity (%)

The diffractograms of the AMC briquettes are plotted in Fig 2, and the identified phases are indicated on the graph along with the JCPDF files used. The major phases of each formulation are corundum (α-$Al_2O_3$) and graphite. From the graph, it is evident that in AMC2 spinel formation begins, and is maximum in AMC6. Relative crystallinity of the individual phases present was calculated with the help of commercially available software OriginLab using the formula:

$$\text{Relative crystallinity (\%)} = \frac{\sum(I\times\beta)desired\ phase}{\sum(I\times\beta)all\ phases} \times 100 \qquad (6.1)$$

Where I is the peak intensity and β is full width at half maximum. Calculations indicate a quantitative phase of the sample have 4.5, 10.7, 21.8, 26.8 and 34.9 % *in-situ* spinel for AMC2, AMC3, AMC4, AMC5 and AMC6 respectively more details are enlisted in Table 6.1. The crystallite size (D), microstrain (ε) and dislocation density (δ) were also evaluated and is listed in Table 6.2.

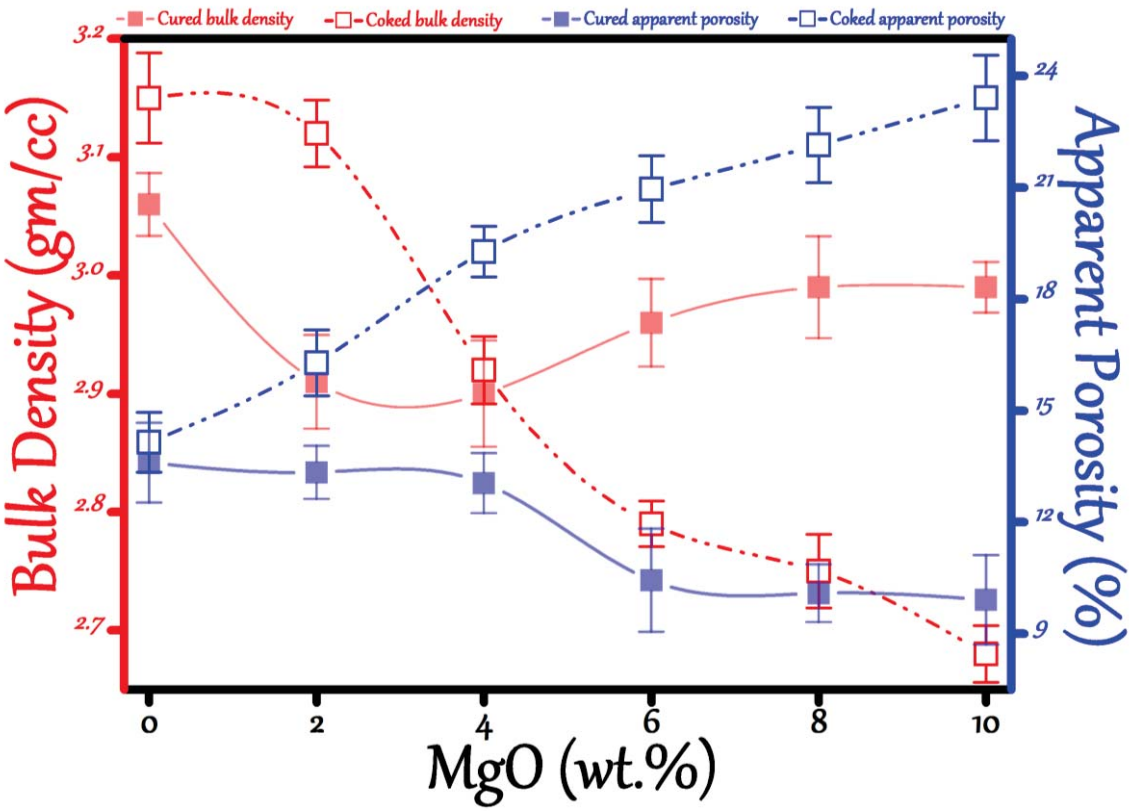


**Fig 6.3** BD and AP of AMC refractories after curing at 200°C and coking at 1400°C

As fine magnesia content increases in the matrix, the AP of cured samples rapidly decreases which becomes almost constant after a 6 wt.% magnesia addition. It brings us to a fact that there is a certain limit to which micro-fine inclusions may help in diminishing the porosity and, in this case, it is 6 wt.% (AMC4). The cured BD initially decreases and then increases which reciprocate the trend followed by coked samples. The formation of new ceramic phase with a lower relative density (spinel) might be the cause for it; this phenomenon is absent in cured samples. The AMC6 has an apparent coked porosity of around 24% owing to in-situ spinelization followed by volumetric expansion. The path taken by the evolution of gaseous products is also responsible for increased coked porosity.

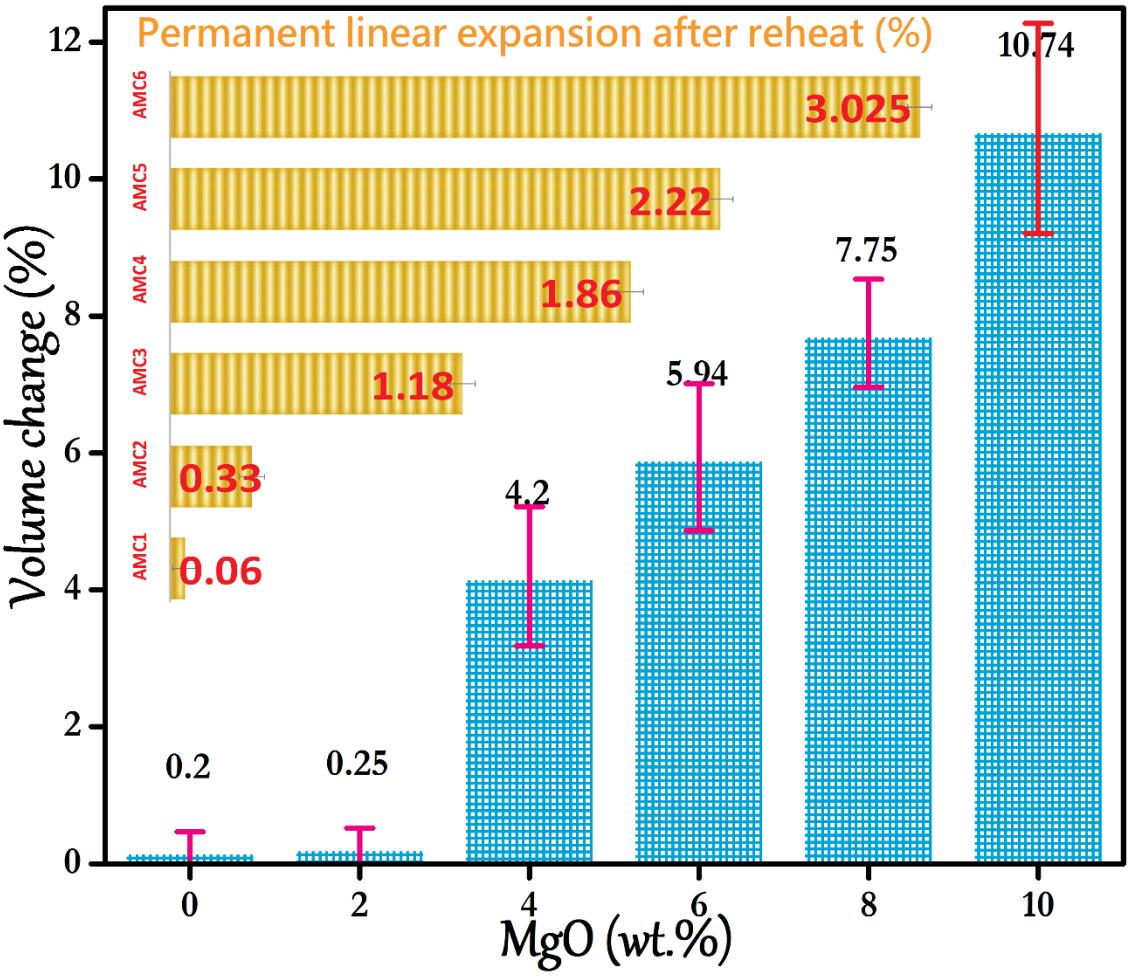


**Fig 6.4** Volumetric expansion and Permanent linear change after one heat cycle as a function of magnesia content

The AMC1 and AMC2 samples show minor volume changes demarcating that alumina, carbon, and rest other do not contribute much to expansion. The samples AMC3-6 illustrates an expansive tendency which confirms that all the expansion is dependent on the amount of magnesia present. The primary contributor to residual expansion is spinel formation, which continues to increase even after reheating. The AMC6 has a PLC value of 3.02%; this huge dramatic expansion may lead to catastrophic failures during use. It also

suggests that other than increasing magnesia content, spinel formation is also dependent on the number of firing cycles or soaking periods.

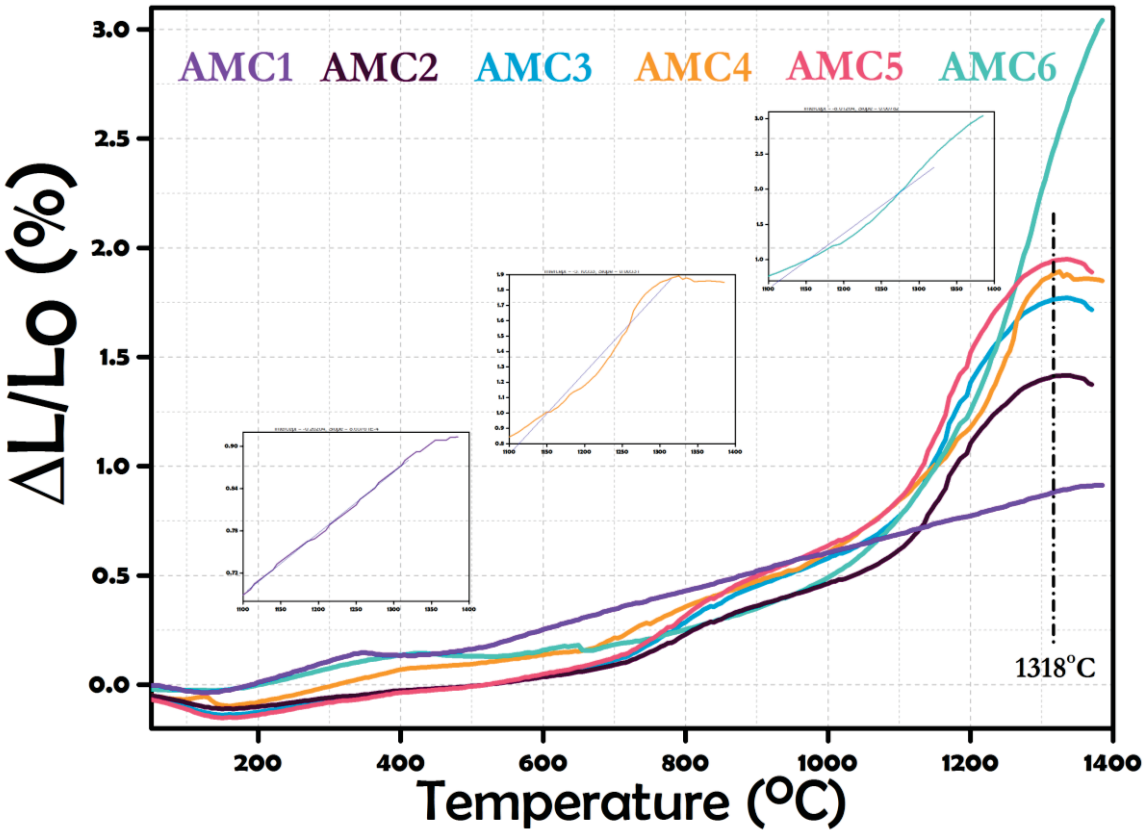


**Fig 6.5** Coefficient of thermal expansion behavior of different AMC refractories; inset figures represent linear fits drawn on AMC1, AMC4, and AMC6

The dilatometric curve of AMC1 is almost linear, progressive and different from rest others. AMC2-5 has a similar incremental slope depending upon the transformations undergone by the materials as the temperature increases. At temperature <200 °C, volumetric contraction occurs in all the six AMC refractories ascribing to resin transformation. It might be well correlated with increased coked density phenomenon. There is another decrement in the slope

of the curves at 650 °C where the glassy carbon starts oxidizing resulting in the formation of gaseous products.

The sudden increase in slope at 1100 °C demarcates that the spinel formation has begun. This expansion can counteract wear on the joints between the refractory bricks. Furthermore, this expansion also results in micro-cracking due to the difference between coefficients of thermal expansion of the product and reagents, which could lead to enforcement mechanisms. However, these micro-cracks can also become entry points for chemically aggressive slags; therefore, the spinel formation reaction must be controlled and the inclusion of magnesia needs to be optimized. The sample AMC2-5 exhibits a negative slope after 1318°C due to liquid phase sintering followed by a quick densification. The inset demonstrates the linear fit of the AMC1, AMC4 and AMC6 curves in the temperature range of 1100-1318°C. The corresponding slopes for AMC1, AMC4 and AMC6 have values $8.65\times10^{-4}°C^{-1}$, $5.31\times10^{-3}°C^{-1}$ and $7.82\times10^{-3}°C^{-1}$ respectively. The AMC6 sample shows abnormally high CTE ascertaining unfit for application viewpoint.

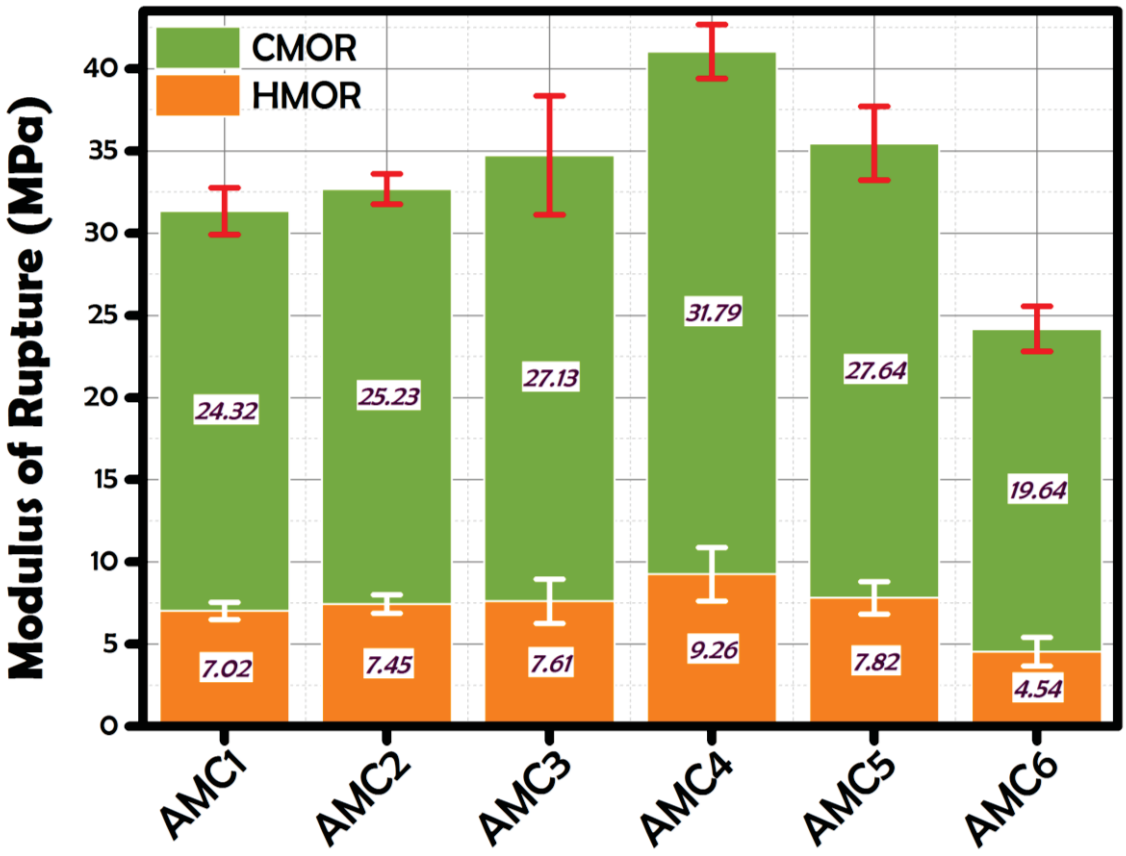


**Fig 6.6** Cold and Hot modulus of rupture of different AMC refractories.

There is a significant 23.4% increase in CMOR value after a 6 wt.% magnesia inclusion although there is a noteworthy decrement after 10 wt.% magnesia addition. Similarly, the HMOR values depict a 24.1% growth and 35.3% decline in AMC4 and AMC6 respectively.

The alumina-based refractories are known to exhibit superplastic behavior at high temperatures in the presence of ultrafine spinel grains. When the temperature was raised, and a tensile stress was applied, the grain boundary sliding might have occurred impeding the abnormal grain growth of alumina thereby increasing the hot strength.

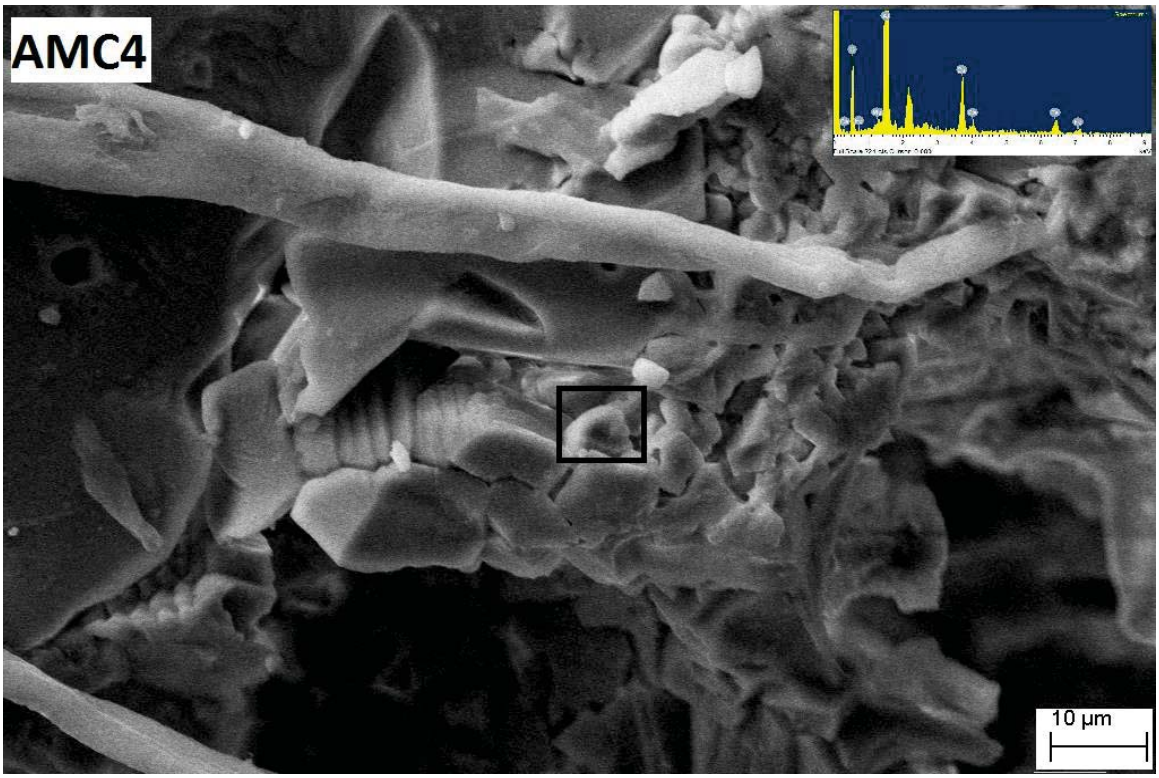


**Fig 6.7 (a)** Microstructure of AMC4

AMC4 has a dense microstructure; free from any visible crack. There is a formation of large whiskers as well which might correspond to *in situ* whiskers of aluminum carbides. The formation of microcracks is visible in AMC6, even though a free expansion might have occurred as it was not lined in a refractory.

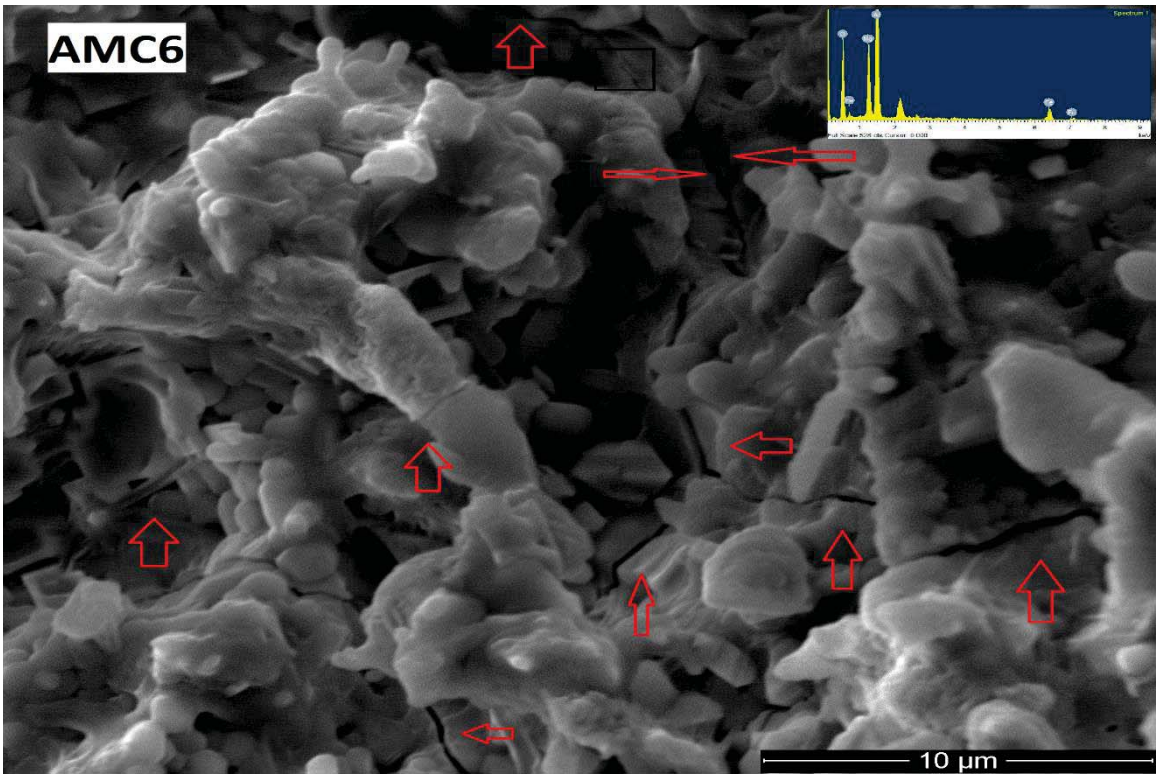


**Fig 6.7 (b)** Microstructure of AMC6

These cracks are inelastic; however, linear thermal expansion is reversible in nature hence upon cooling the joint structure will tend to open. So for a successful lining, it would be wise to use lower amounts of magnesia. EDX analysis in the inset mark the existing elements in the right proportion, indicating that the specimen is primarily composed of aluminum, magnesium, oxygen and carbon.

### 6.4 Summary of Results

The work in this chapter proposes a comprehensive approach to evaluating the limiting value of magnesia in $Al_2O_3$-MgO-C refractory. The thermal analysis distinguishes the weight loss from the combustion of the resin. The X-ray

diffraction has proven to be a simple, practical and accurate tool for the quantitative determination of the mineralogical composition. The density and porosity are found to be dependent on micro-fine additions and *in situ* spinelization. Linear dimensional changes continue to occur after reheat and dilatometric analysis establish that its chief cause is spinel formation. The structural defects in AMC6 by forming of $MgAl_2O_4$ lead to continuous crack which further result in the destruction of the sample by load bearing stress at high temperature.